



# Journal of Applied and Computational Mechanics



Research Paper

## MHD Casson Nanofluid Past a Stretching Sheet with the Effects of Viscous Dissipation, Chemical Reaction and Heat Source/Sink

G. Narender<sup>1</sup>, K. Govardhan<sup>2</sup>, G. Sreedhar Sarma<sup>1</sup>

<sup>1</sup> Department of Humanities and Sciences (Mathematics), CVR College of Engineering, Hyderabad-501510, Telangana State, India

<sup>2</sup> Department of Mathematics, GITAM University, Hyderabad-502329, Telangana State, India

Received August 08 2019; Revised September 27 2019; Accepted for publication October 09 2019.

Corresponding author: G. Narender (gnriimc@gmail.com)

© 2020 Published by Shahid Chamran University of Ahvaz

**Abstract.** The effects of viscous dissipation, chemical reaction and activation energy on the two-dimensional hydromagnetic convective heat and mass transfer flow of a Casson nanofluid fluid over a stretching sheet with thermal radiation, have been discussed in detail. The formulated highly nonlinear equations for the above-mentioned flow are converted into first-order ordinary differential equations (ODEs). The shooting method along with Adams-Bashforth Moulton method is used to solve the BVP by using the Fortran language program. The numerical results are computed by choosing different values of the involved physical parameters and compared with earlier published results and excellent validation of the present numerical results has been achieved for local Nusselt number and local Sherwood number. The graphical numerical results of different physical quantities of interest are presented to analyze their dynamics under the varying physical quantities. From the results, it has been remarked that the heat transfer rate escalates for the large values of radiation parameter, viscous dissipation for the Casson nanofluid.

**Keywords:** Casson nanofluid, Viscous dissipation, Chemical reaction, Brownian motion, Thermophoresis, Stretching Sheet.

### 1. Introduction

Nanofluids are processed by the diffusion of the suspended nanoparticles in the immersed liquid (a base fluid and nanoparticles). Moreover, such fluids when compared with the conventional heat transfer fluids, have a much higher rate of thermal conduction and exhibit significant characteristics. Owing to their enhanced features, nanofluids have immense applications in the automobile industries, medical arena, power plant cooling systems, nuclear engineering and a lot more. Moreover, several research studies have been performed by considering the different aspects of the flows past a stretching sheet. Crane [1] discussed the flow by considering a stretching sheet. Pavlov [2] illustrated his findings on the MHD flow past a stretching sheet. On the contrary, Fang and Zhang [3] explored the MHD flow past a stretching sheet by examining the wall mass suction and presented the exact solution for the problem. In addition, many significant features of the MHD flow past a stretching sheet were presented and elaborated in the literature [4-7].

Anjali Devi and Ganga [8] studied the MHD flow over a porous stretching sheet under the influence of Joule heating and viscous dissipation. Makinde and Mutuku [9] investigated the thermal boundary layer of hydromagnetic nanofluids over a heated plate under the impact of Ohmic heating and viscous dissipation. Ahmed et al. [10] investigated the impacts of heatsink/source on the boundary layer flow of single-phase nanofluid over a stretching tube. Very recently, Akilu and Narahari [11] studied numerically the impact of internal heat absorption of a nanofluid on natural convective flow over an inclined plate numerically.

Furthermore, other types of fluids have been used for describing the different flow problems, which are not non-Newtonian in nature and are regarded as Newtonian fluids. In the past few years, the problem involving stagnation point flow has acquired the considerable attention of many research scientists. Owing to its significant properties, the study of flow nearby a stagnation point past a stretching/shrinking sheet has a wide range of practical applications, for instance, cooling process of atomic reactors and electronic equipment, the layouts of thrust bearings, and several hydrodynamics processes. Moreover, the analysis of the magnetohydrodynamic flow is highly significant in the fluid dynamics owing to the reason that the impact of the magnetic field on the viscous flow using a fluid having electrically conducting properties has played a key role in several commercial productions, for instance in the refinement of crude oil, glass, and paper production, manufacturing of magnetic materials, geophysics and MHD electrical power generation. The MHD factor has a fundamental role to play in controlling the cooling rate and for achieving the desired quality of the product. Mahapatra [12] analyzed the flow nearby a stagnation point by taking into consideration the heat transfer past a stretching sheet. Furthermore, Nazar et al. [13] discussed the stagnation point flow over a stretching sheet using a micropolar fluid. Several researchers have contributed to the study of the stagnation point MHD flow in the light of various significant effects [14-18].

Fluids serve as the necessity of life and owing to their significance in natural and technological processes, scientists have been discovering the various facts and figures about the fluid flow. Fluid dynamics characterizes the flow of fluids and how forces



influence them. It illustrates the methodology of understanding the evolution of stars, meteorological phenomena, marine currents as well as the blood circulation. Archimedes was a Greek mathematician, who first examined the statics and buoyancy of the fluid and formulated the Archimedes principle, which was the first contribution in the area of fluid mechanics. Rapid investigation on this subject began in the fifteenth century. Some crucial engineering applications of fluid dynamics comprise oil pipelines, rocket engines, air conditioning systems, and wind turbines. Casson fluid, being non-Newtonian in nature, exhibits the behavior of elastic solids. When stress rate is zero, the Casson fluid can be regarded as a shear-thinning liquid, showing an infinite viscosity whereas the viscosity drops to zero as the stress rate approaches an infinite value [19]. Jam, tomato ketchup, honey and concentrated fruit syrups are some familiar examples of the Casson fluid. The Casson fluid has been implemented in the preparation of printing ink, silicon suspensions and polymers [20]. During the past few years, a vast range of experiments and investigations have been carried out using the Casson fluid due to its enormous applications in the scientific and engineering domains. Dash et al. [19] examined the flow using a homogeneous porous medium inside a pipe for the Casson fluid. The stagnation point flow for mixed convection and convective boundary conditions using the Casson fluid was analyzed by Hayat et al. [21]. Further to this, Mukhopadhyay et al. [22] investigated the flow past an unsteady stretching surface using the Casson fluid. Moreover, the aspects of such flows using the Casson fluid are presented in recent studies [23–30].

The leading motivation for the present work is to investigate the impacts of external magnetic field inclinations and viscous dissipation due to heat generation or absorption parameter on MHD mixed convective flow of Casson nanofluid. Moreover, the chemical reaction and radiation effects are examined. The governing partial differential equations (PDEs) have been converted to a set of ODEs through suitable similarity transformations and the numerical solution has been derived by the shooting technique with Adams – Bashforth Moulton method of order four.

## 2. Mathematical Model of the Flow

The present model aims to investigate the laminar, incompressible, 2D and steady flow of the Casson nanofluid past a stretched surface. Along the x-axis, a stretching sheet is taken with stretching velocity  $u_w = ax$  where the fluid flow is bounded by the region  $y > 0$ . In the light of thermal radiation and heat generation/absorption, the characteristics of flow and heat transfer are examined. The temperature provided to the stretching surface is denoted by  $T_f$ , with  $h_f$  as the heat transfer coefficient,  $C_w$  as surface concentration.  $C_\infty$  denotes the ambient concentration and  $T_\infty$  represents the ambient temperature. With the assumption that no nanoparticles flux is present on the surface, the impact of thermophoresis is incorporated along with boundary conditions. A magnetic field is applied normal to the stretching surface having strength  $B_0$  as we can see in Figure 1 induced magnetic field is ignored with the assumptions of small values of magnetic Reynolds number. The rheological equation of state for an isotropic and incompressible flow of a Casson fluid is

$$\tau_{ij} = \begin{cases} 2 \left( \mu_b + \frac{p_y}{\sqrt{2\pi}} \right) e_{ij}, \pi > \pi_c \\ 2 \left( \mu_b + \frac{p_y}{\sqrt{2\pi_c}} \right) e_{ij}, \pi_c > \pi \end{cases} \quad (1)$$

In the above expression where  $\mu_b$  is the plastic dynamic viscosity of the non-Newtonian fluid,  $p_y$  is the yield stress of fluid,  $\pi$  is the product of the component of deformation rate and itself, namely,  $\pi = e_{ij} e_{ij}$ ,  $e_{ij}$  is the (i, j) component of the deformation rate, and  $\pi_c$  is a critical value of  $\pi$  based on the non-Newtonian model.

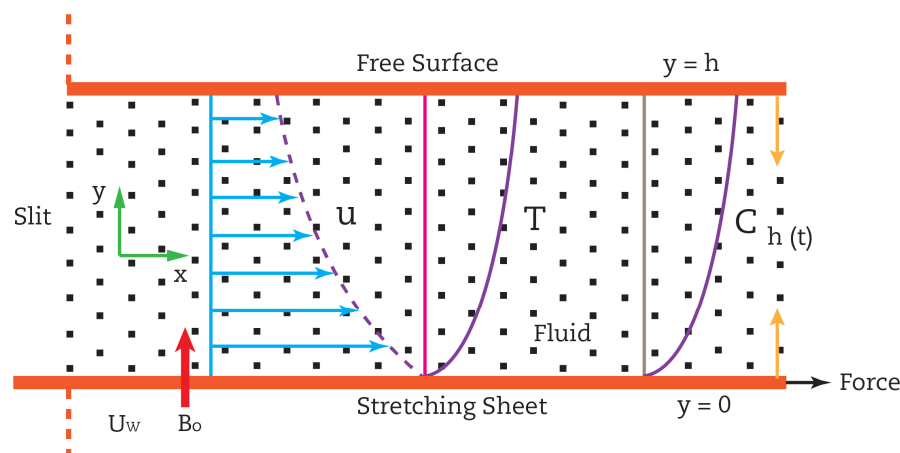


Fig. 1. Geometry for the flow under consideration.

The constitutive equations of the Casson nanofluid model are as follow [31]:

The Continuity equation:

$$\frac{\partial u}{\partial x} + \frac{\partial v}{\partial y} = 0 \quad (2)$$

The Momentum equation:



$$\frac{\partial u}{\partial x}u + \frac{\partial v}{\partial y}v = -\frac{\sigma^* B_0^2}{\rho}u + v \left( 1 + \frac{1}{\beta} \right) \left( \frac{\partial^2 u}{\partial x^2} + \frac{\partial^2 u}{\partial y^2} \right) + g\beta_T (T - T_\infty) + g\beta_C (C - C_\infty) \quad (3)$$

The Energy equation:

$$\frac{\partial T}{\partial x}u + \frac{\partial T}{\partial y}v = -\frac{\mu}{\rho C_p} \left( 1 + \frac{1}{\beta} \right) \left( \frac{\partial u}{\partial y} \right)^2 + \alpha \left( \frac{\partial^2 T}{\partial x^2} + \frac{\partial^2 T}{\partial y^2} \right) - \frac{1}{\rho C_p} \frac{\partial q_r}{\partial y} + \tau \left\{ D_B \left( \frac{\partial C}{\partial x} \frac{\partial T}{\partial x} + \frac{\partial C}{\partial y} \frac{\partial T}{\partial y} \right) + \frac{D_T}{T_\infty} \left( \frac{\partial T}{\partial y} \right)^2 + \left( \frac{\partial T}{\partial x} \right)^2 \right\} - \frac{Q}{\rho C_p} (T - T_\infty) \quad (4)$$

The Concentration equation:

$$\frac{\partial C}{\partial x}u + \frac{\partial C}{\partial y}v = D_B \left( \frac{\partial^2 C}{\partial x^2} + \frac{\partial^2 C}{\partial y^2} \right) - \frac{D_T}{T_\infty} \left( \frac{\partial^2 T}{\partial x^2} + \frac{\partial^2 T}{\partial y^2} \right) - k_1 (C - C_\infty) \quad (5)$$

The corresponding boundary conditions for the proposed model are

$$u = U_w(x) \Rightarrow u = ax, v = 0, -k \frac{\partial T}{\partial y} = h(T_f - T), -D \frac{\partial C}{\partial y} = h^*(C_f - C) \text{ at } y = 0 \quad (6a)$$

$$u = 0, v = 0, T \rightarrow T_\infty, C \rightarrow C_\infty \text{ as } y \rightarrow \infty \quad (6b)$$

In the above equations,  $\sigma^*$  is electrical conductivity of the base fluid,  $B_0$  is the uniform magnetic field strength,  $g$  is the gravitational acceleration,  $\beta = \sqrt{2\pi} \mu_B / p_y$  is the Casson parameter,  $\nu = \mu_B / \rho$  is the kinematics viscosity,  $\alpha$  is the thermal diffusivity,  $k$  is the thermal conductivity,  $\tau$  is the ratio of nanoparticle heat capacity and base fluid capacity,  $D_B$  is the Brownian diffusion coefficient,  $D_T$  is the thermophoresis diffusion coefficient,  $\beta_T$  volumetric thermal expansion coefficient,  $\beta_C$  is volumetric solutal thermal expansion coefficient,  $x$  and  $y$  are coordinate axis along the continuous surface in the direction same as direction of motion and normal to it, respectively. The components of velocity along  $x$  – and  $y$  – axis are respectively  $u$  and  $v$ ,  $U_B$  is the stretching velocity,  $U$  is the uniform velocity.

The velocity components in terms of the stream functions are given as

$$u = \frac{\partial \psi}{\partial y}, v = -\frac{\partial \psi}{\partial x} \quad (7)$$

In Eq. (4), the Rosseland approximation for heat flux  $q_r$  is given as

$$q_r = \frac{-4\sigma^*}{3k^*} \frac{\partial T^4}{\partial y} \quad (8)$$

where  $k^*$  stand for the absorption coefficient and  $\sigma^*$  Stefan-Boltzmann constant. If temperature constant is very small, then  $T^4$  might be expanded about  $T_\infty$  by utilizing Taylor series, given as:

$$T^4 = T_\infty^4 + \frac{4T_\infty^3}{1!}(T - T_\infty) + \frac{12T_\infty^2}{2!}(T - T_\infty)^2 + \frac{24T_\infty}{3!}(T - T_\infty)^3 + \dots \quad (9)$$

Higher order terms are ignored resulting in the following form:

$$T^4 = T_\infty^4 + 4T_\infty^3(T - T_\infty) \Rightarrow T^4 = T_\infty^4 + 4T_\infty^3 T - 4T_\infty^4 \Rightarrow T^4 = 4T_\infty^3 T - 3T_\infty^4 \\ \Rightarrow \frac{\partial T^4}{\partial y} = 4T_\infty^3 \frac{\partial T}{\partial y} \quad (10)$$

Using Eq. (10) in Eq. (8) and differentiating, the following form is achieved:

$$\frac{\partial q_r}{\partial y} = -\frac{16\sigma^* T_\infty^3}{3k^*} \frac{\partial^2 T}{\partial y^2} \quad (11)$$

To solve the above system of PDEs numerically, it is converted into the nondimensionalized form. For this, the following dimensionless variables are used:

$$\psi = \sqrt{avx} f(\eta), \eta = y \sqrt{\frac{a}{v}}, \theta(\eta) = \frac{T - T_\infty}{T_f - T_\infty}, \phi(\eta) = \frac{C - C_\infty}{C_w - C_\infty} \quad (12)$$

The above, equation (2) is satisfied identically. After using similarity transformation, the equations take the form

$$\left( 1 + \frac{1}{\beta} \right) f'' + ff'' - (f')^2 - Mf' + \lambda(\theta + N\phi) = 0 \quad (13)$$

$$\left( 1 + \frac{4}{3}R \right) \theta'' + Pr \left( f\theta' + Nb\phi'\theta' + Nt(\theta')^2 + \left( 1 + \frac{1}{\beta} \right) Ec(f'')^2 + \beta_1 \theta \right) = 0 \quad (14)$$



$$\varphi'' + Sc \varphi' + \frac{Nt}{Nb} \theta'' - Sc \gamma \varphi = 0 \quad (15)$$

The BCs, now, become:

$$\left. \begin{aligned} f(0) = 0, f'(0) = 1, \theta'(0) = -\gamma_1[1 - \theta(0)], \varphi'(0) = -\gamma_2[1 - \varphi(0)] \text{ at } y = 0 \\ f'(\infty) \rightarrow 0, \theta(\infty) \rightarrow 0, \varphi(\infty) \rightarrow 0 \text{ as } \eta \rightarrow \infty \end{aligned} \right\} \quad (16)$$

The dimensionless parameters are defined as

$$\begin{aligned} \lambda = \frac{Gr_x}{Re_x^2}, Sc = \frac{\nu}{D}, Gr_x = \frac{g\beta_T(T_f - T_\infty)x^3}{\nu^2}, M = \frac{\sigma B_0^2(x)}{\rho}, Nt = \frac{\beta_c(C_w - C_\infty)}{\beta_T(T_w - T_\infty)}, R = \frac{4\sigma T_\infty^3}{k_0 k} \\ Pr = \frac{\nu}{\alpha}, Nb = \frac{\rho_p D_B(C_w - C_\infty)}{\rho_f \alpha}, Ec = \frac{u^2}{c_p(T_f - T_\infty)}, \gamma = \frac{k_1}{a}, \beta_1 = \frac{Q}{\rho c_p}, \gamma_1 = \frac{h}{k} \sqrt{\frac{\nu}{a}}, \gamma_2 = \frac{h^*}{k} \sqrt{\frac{\nu}{a}}, \end{aligned} \quad (17)$$

The skin friction coefficient  $C_f$ , Nusselt number  $Nu_x$  and Sherwood number  $Sh_x$  are defined as

$$C_f = \frac{\tau_w}{\rho u_w^2}, Nu_x = \frac{x q_w}{k(T_w - T_\infty)}, Sh_x = \frac{x h_w}{D_B(\varphi_w - \varphi_\infty)} \quad (18)$$

Here, the heat flux  $q_w$ , the skin - friction on flat plate  $\tau_w$  and the mass transfer rate  $h_w$  are given by

$$q_w = -k \left( \frac{\partial T}{\partial y} \right)_{y=0}, \tau_w = \left( \mu_B + \frac{p_y}{\sqrt{2\pi}} \right) \left( \frac{\partial u}{\partial y} \right)_{y=0}, h_w = -D_B \left( \frac{\partial \varphi}{\partial y} \right)_{y=0} \quad (19)$$

By using the above equations:

$$C_f \sqrt{Re_x} = \delta \left( 1 + \frac{1}{\beta} \right) f''(0), \frac{Nu_x}{\sqrt{Re_x}} = \theta'(0), \frac{Sh_x}{\sqrt{Re_x}} = \varphi'(0) \quad (20)$$

Here,  $Re_x = U_w x / \nu$  is the local Reynold number.

### 3. Numerical Treatment

The numerical solution of the mathematical model in the form of non-linear differential equations (13-15) along with the boundary condition (16) was reported by Hayat et al. [31]. They opted the series solution for the numerical solution of the above model. In the present section, shooting technique has been proposed to reproduce the same solution. The Adams-Bashforth Moulton method of order four and the Newton's technique for solving the non-linear algebraic equations, are the main components of the shooting technique. By re-writing equation (13-15) as:

$$f'' = \frac{-1}{\left(1 + \frac{1}{\beta}\right)} \left[ f f'' - (f')^2 - M f' + \lambda(\theta + N \varphi) \right] \quad (21)$$

$$\theta'' = \frac{Pr}{\left(1 + \frac{4}{3}R\right)} \left[ f \theta' + Nb \varphi' \theta' + Nt (\theta')^2 + \left(1 + \frac{1}{\beta}\right) Ec (f')^2 + \beta_1 \theta \right] \quad (22)$$

$$\varphi'' = - \left[ Sc \varphi' + \frac{Nt}{Nb} \theta'' - Sc \gamma \varphi \right] \quad (23)$$

To have a system of first order ODEs, use the notations:

$$f = y_1, f' = y_2, f'' = y_3, \theta = y_4, \theta' = y_5, \varphi = y_6, \varphi' = y_7 \quad (24)$$

By using the notations (24), we the following IVP:

$$\left. \begin{aligned} y_1' &= y_2, & y_1(0) &= 0, \\ y_2' &= y_3, & y_2(0) &= 1, \\ y_3' &= -\frac{1}{\left(1 + \frac{1}{\beta}\right)} \left[ y_2^2 + M y_2 - y_1 y_3 - \lambda(y_4 + N y_6) \right], & y_3(0) &= r, \\ y_4' &= y_5, & y_4(0) &= 0, \\ y_5' &= -\frac{Pr}{\left(1 + \frac{4}{3}R\right)} \left[ y_1 y_5 + N b y_7 y_5 + N t y_5^2 + E c y_3^2 + \beta_1 y_4 \right], & y_5(0) &= \gamma_1(s-1), \\ y_6' &= y_7, & y_6(0) &= t, \\ y_7' &= -Sc y_1 y_7 - \frac{Nt}{Nb} y_5' + Sc \gamma y_6, & y_7(0) &= \gamma_2(t-1). \end{aligned} \right\} \quad (25)$$



where  $r$ ,  $s$  and  $t$  are the initial guesses. For the computational purpose, the unbounded domain  $[0, \infty)$  has been replaced by a bounded domain  $[0, \eta_\infty]$ , where  $\eta_\infty$  is some suitable finite real number. It is chosen in such a way that the solutions of the problem start looking settled for  $\eta > \eta_\infty$ . In (25), the missing initial conditions  $r$ ,  $s$  and  $t$  are to be chosen such that

$$y_2(\eta_\infty, r, s, t) = 0, y_4(\eta_\infty, r, s, t) = 0, y_6(\eta_\infty, r, s, t) = 0 \quad (26)$$

To start the iterative process, choose  $r = r_0$ ,  $s = s_0$  and  $t = t_0$ . To the values of  $r$ ,  $s$  and  $t$  Newton's iterative scheme has been used.

$$d^* = e^* - f^* g \quad (27)$$

where

$$d^* = \begin{pmatrix} r^{(n+1)} \\ s^{(n+1)} \\ t^{(n+1)} \end{pmatrix}, e^* = \begin{pmatrix} r^{(n)} \\ s^{(n)} \\ t^{(n)} \end{pmatrix}, f^* = \begin{bmatrix} \frac{\partial y_2}{\partial r} & \frac{\partial y_2}{\partial s} & \frac{\partial y_2}{\partial t} \\ \frac{\partial y_4}{\partial r} & \frac{\partial y_4}{\partial s} & \frac{\partial y_4}{\partial t} \\ \frac{\partial y_6}{\partial r} & \frac{\partial y_6}{\partial s} & \frac{\partial y_6}{\partial t} \end{bmatrix}_{\eta_\infty, r^{(n)}, s^{(n)}, t^{(n)}}^{-1}, g = \begin{pmatrix} y_2^{(n+1)} \\ y_4^{(n+1)} \\ y_6^{(n+1)} \end{pmatrix} \quad (28)$$

The convergence criteria are chosen to be successive value agree up to 3 significant digits. The choice  $\eta_{\max} = 9$  was more than enough for end conditions.

## 4. Results and Discussion

In this section, the numerical values of Nusselt number and Sherwood numbers are illustrated by tables and graphs by assuming varies values of different physical parameters of interest.

### 4.1 Code validation

To validate the computational program language Fortran code the values of  $-\theta'(0)$  and  $-\phi'(0)$  are reproduced for the problem discussed by [31]. Table 4.1 reflects a very good agreement between the results computed by the present code and the code in [31]. In Table 4.2, numerical analysis of physical parameters such as mixed convection parameter  $\lambda$ , concentration buoyancy parameter  $N$ , heat transfer Biot number  $\gamma_1$  and mass transfer Biot number  $\gamma_2$  and their influence on local Nusselt and Sherwood numbers is presented. From this table, it is noted that an increase in the mixed convection parameter and concentration buoyancy parameter, the Nusselt number increases whereas the Sherwood number decreases.

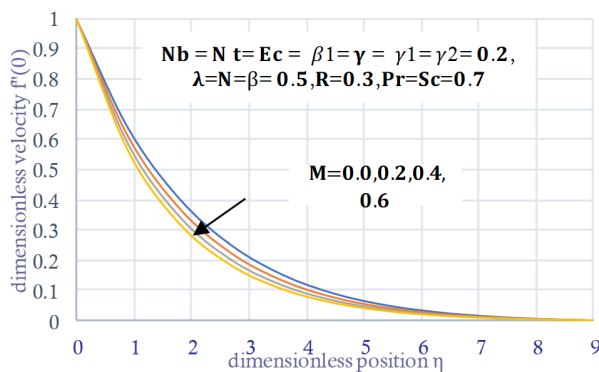


**Fig. 2.** Variation of  $M$  on  $f'(\eta)$

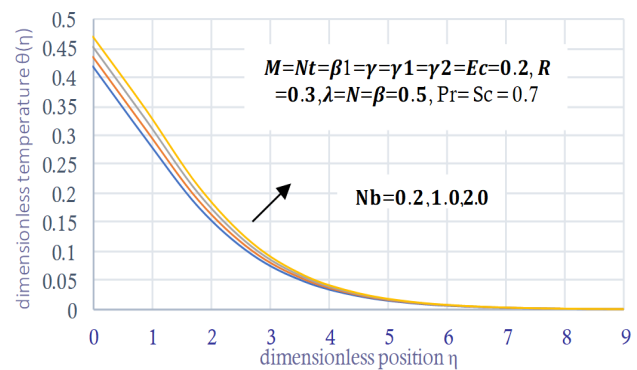


**Fig. 3.** Variation of  $Nb$  on  $\theta(\eta)$

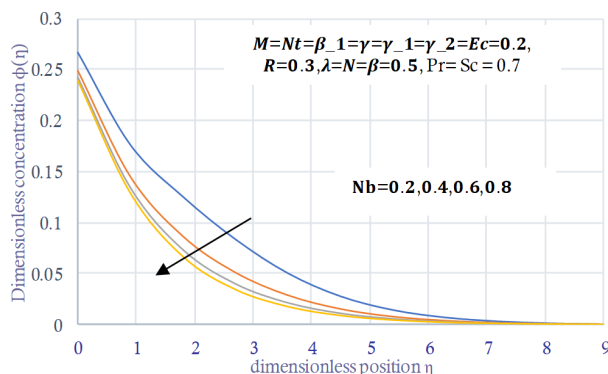


**Fig. 4.** Variation of  $Nb$  on  $\phi(\eta)$

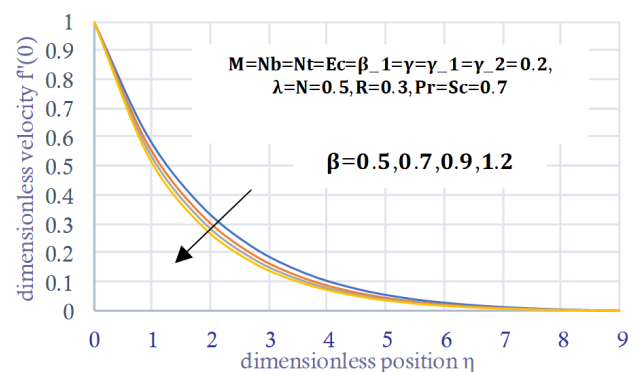


**Fig. 5.** Variation of  $\beta$  on  $f'(\eta)$

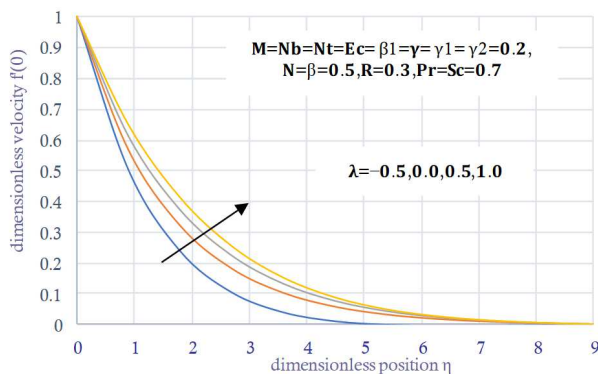
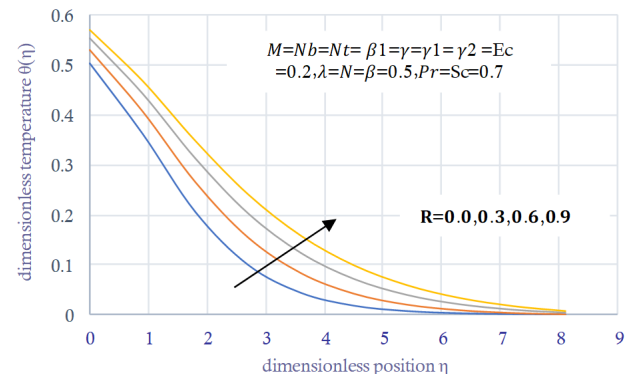
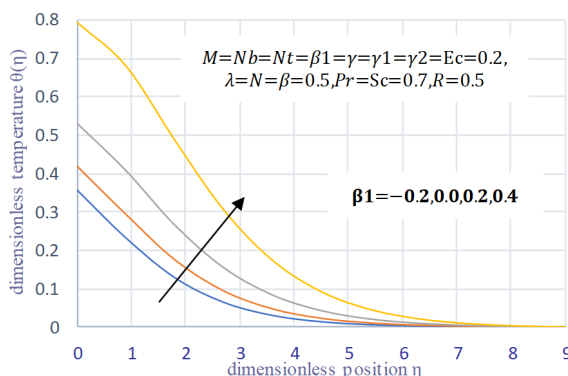
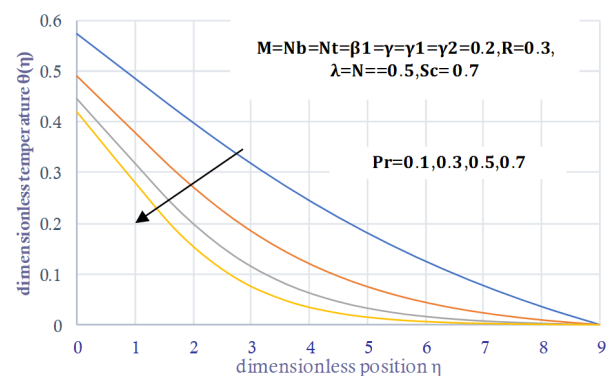


**Table 4.1.** Comparison of current code results with some earlier results of [28].

$\beta$	$Nt$	$Nb$	$-\theta'(0)$		$-\phi'(0)$	
			T. Hayat et al. [31]	Present Result	T. Hayat et al. [31]	Present Result
0.5	0.2	0.2	0.15271	0.1526939	0.12054	0.1205407
	0.7		0.15204	0.1519901	0.11910	0.1188185
	0.9		0.15150	0.1514782	0.11758	0.1175741
0.5	0.4		0.15195	0.1518633	0.096142	0.0956810
	0.6		0.15106	0.1510139	0.071520	0.0717563
		0.4	0.15186	0.1517981	0.13368	0.1336129
		0.6	0.15100	0.1509065	0.13815	0.1379848

**Table 4.2.** Comparison of current results of  $-\theta'(0)$  and  $-\phi'(0)$  for numerous values of  $Nt$  &  $Nb$ .

$\lambda$	$N$	$\gamma_1$	$\gamma_2$	$-\theta'(0)$		$-\phi'(0)$	
				T. Hayat et al. [31]	Present Result	T. Hayat et al. [31]	Present Result
-0.5	0.3	0.2	0.2	1.5201	0.1411910	0.11969	0.0840725
0.0				0.15248	0.1524246	0.12014	0.1199470
0.3				0.15271	0.1526939	0.12054	0.1205407
0.6				0.15302	0.1529436	0.12144	0.1210837
0.3	0.0			0.15261	0.1525648	0.12032	0.1202398
	0.3			0.15271	0.1526939	0.12054	0.1205407
	0.6			0.15302	0.1528177	0.12078	0.1208268
0.3	0.3	0.2		0.15271	0.1526939	0.12054	0.1205407
		0.4		0.24602	0.2458604	0.10535	0.1053597
		0.6		0.30822	0.3080297	0.095273	0.0954224
0.3	0.3	0.2	0.1	0.15304	0.1529687	0.069638	0.0694951
			0.3	0.15255	0.1524822	0.15995	0.1599500
			0.5	0.15224	0.1521774	0.21584	0.2156148

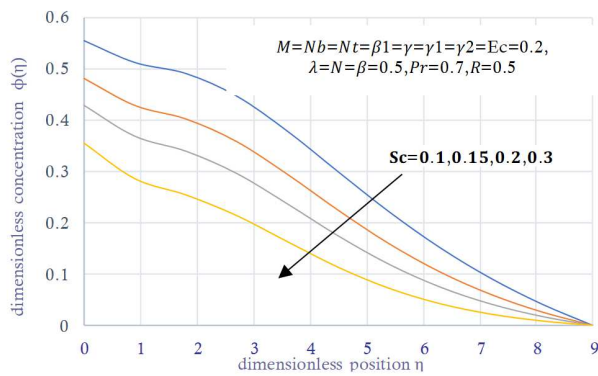
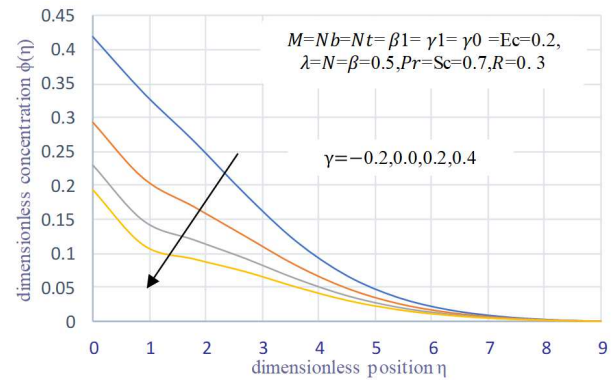
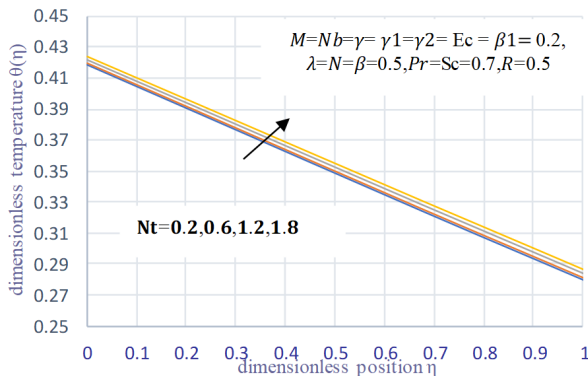
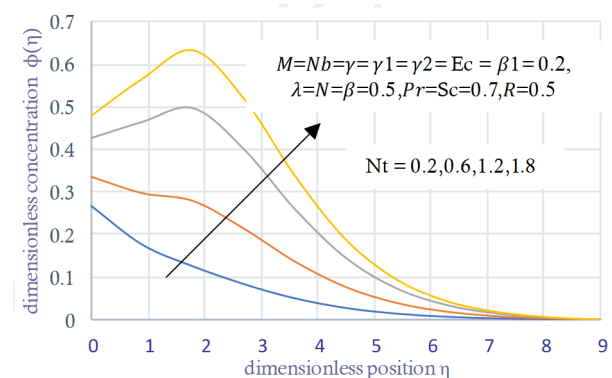
**Fig. 6.** Variation of  $\lambda$  on  $f(\eta)$ **Fig. 7.** Variation of  $R$  on  $\theta(\eta)$ **Fig. 8.** Variation of  $\beta_1$  on  $\theta(\eta)$ **Fig. 9.** Variation of  $Pr$  on  $\theta(\eta)$ 

## 4.2 The velocity, Temperature and Concentration profiles

The graphs illustrated in this section show the behavior of the velocity, temperature and concentration for the present model regarding a change in the values of various parameters like  $M, Nb, \beta, \lambda, R, Pr, Sc, \beta_1, Nt, \gamma_1, \gamma, Ec$ . Figure 2 presents the impact of the magnetic parameter on the velocity distribution. From this figure, with increasing values of the magnetic parameter, the profile of velocity decreases. The reason beyond this electrically conducting fluid produces a resistive force known as Lorentz force, which opposes the flow and tends to make the fluid motion slowdown in the boundary layer and therefore reduces the profile of velocity.





Fig. 10. Variation of  $Sc$  on  $\phi(\eta)$ Fig. 11. Variation of  $\gamma$  on  $\phi(\eta)$ Fig. 12. Variation of  $Nt$  on  $\theta(\eta)$ Fig. 13. Variation of  $Nt$  on  $\phi(\eta)$ 

Figures 3-4 display the influence of the Brownian motion parameter on the temperature and concentration distributions. The temperature profile climbs marginally for the larger values of  $Nb$ . This happens due to the reason that as the value of  $Nb$  rises, the movement of the nanoparticles enhances significantly which triggers the kinetic energy of the nanoparticles resulting in an escalation in the temperature and the thermal boundary layer thickness. On the other hand, the concentration of the fluid falls as  $Nb$  assumes the higher values. Also, the concentration boundary layer thickness is depressed.

Figure 5 is framed to delineate the effect of the Casson parameter on the velocity field. The velocity profile shows an increasing trend by increasing  $\beta$ . Additionally, the velocity boundary layer thickness undergoes a decrement as  $\beta$  assumes the larger value. This stems from the fact that the plasticity of the Casson fluid increases for the smaller  $\beta$  and leads to an enhancement in the momentum boundary layer thickness.

Figure 6 depicts the effect of the mixed convection parameter on the velocity. It is seen that as  $\lambda$  increases, the velocity increases. This is because the positive force acts like a favorable pressure gradient and hence accelerates the fluid flow in the boundary layer. This results in higher velocity as  $\lambda$  increases.

Figures 7 & 8 elucidate the effect of the radiation parameter  $R$  and the heat generation or absorption parameter  $\beta_1$  on the temperature distributions. Since the heat transfer climbs marginally for the higher estimation of  $R$ , thereby an increment in the temperature of the fluid and the thermal boundary layer has been noticed. However, as the value of  $\beta_1$  rises, more heat is generated causing an increment in the temperature and the thermal boundary layer thickness. On the other hand, as the value of  $\beta_1$  de-escalates, the heat absorbed results in a decrement in the temperature and the associated thermal boundary layer thickness.

Figure 9 is framed to delineate the outcome of  $Pr$  on temperature distribution. Since  $Pr$  is directly proportionate to the viscous diffusion rate and inversely related to the thermal diffusivity, so the thermal diffusion rate suffers a reduction for the larger estimation of  $Pr$  and subsequently, the temperature of the fluid drops significantly. Moreover, a decrement in the thermal boundary layer thickness has been noted.

Figures 10 & 11 delineate the outcome of  $Sc$  and  $\gamma$  on the concentration fields. The concentration of the fluid depicts a decreasing behavior as  $Sc$  assumes a higher value. This behavior stems from the fact that the Schmidt number and mass diffusion rate have inverse relation, therefore, for the larger  $Sc$ , the process of the mass diffusivity slows down and thus, the concentration falls, and the concentration boundary layer thickness is reduced. Furthermore, the chemical reaction parameter also has a similar effect on the concentration profile. The larger values of  $\gamma$  result in a decrement in the chemical molecular diffusion and hence, the concentration of the fluid de-escalates, and the associated concentration boundary layer thickness is reduced.

Figures 12 & 13 interpret the impact of the thermophoresis parameter on the temperature and concentration distributions. Both the temperature and concentration escalate by taking larger values of  $Nt$  into account. In addition to this, an increment in the associated thermal and concentration boundary layer has been noticed. Physically, heated particles come away from high temperature as compared to low-temperature so the temperature of fluid increases.

Figures 14 and 15 are presented to visualize the effect of the  $\gamma_1$  on temperature distribution and concentration profile. This figure defines that temperature profile and concentration profile enhances as the Biot number  $\gamma_1$  is increased gradually. Physically, the Biot number defines the ratio between the resistance rate of heat transfer inside the body to the resistance at the body surface. The reason behind is that convective heat exchange at the surface will raise the boundary layer thickness therefore the nanofluid with convective boundary condition is a more effective model as compared to the constant surface temperature estate.



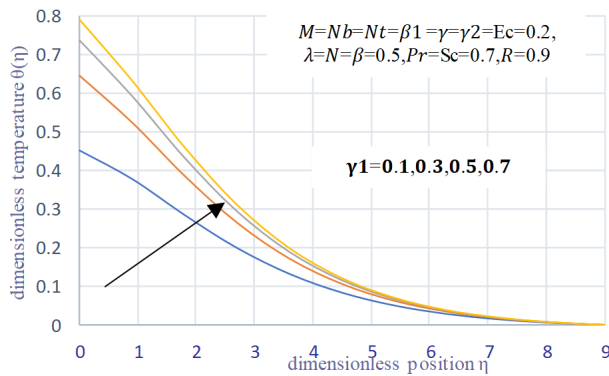
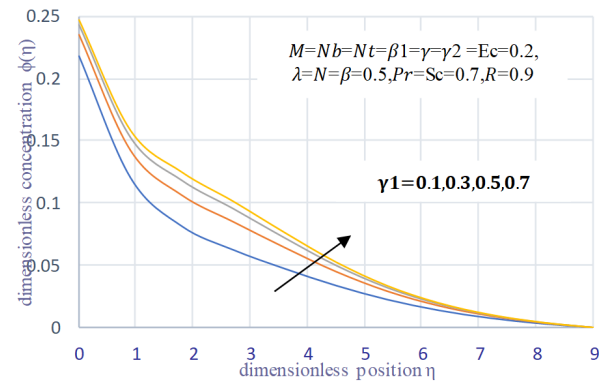
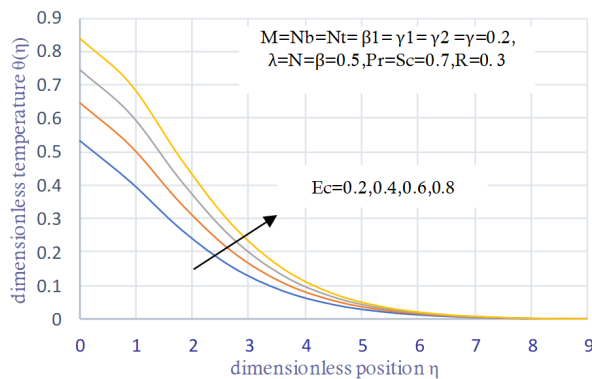
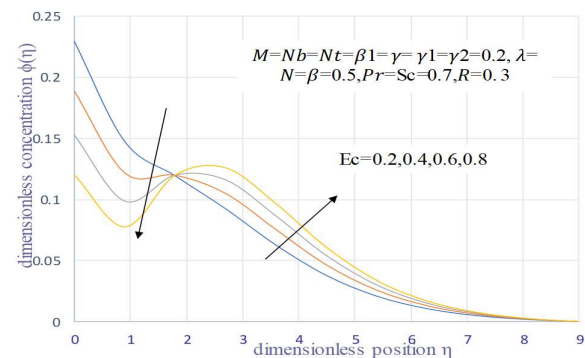
Fig. 14. Variation of  $\gamma_1$  on  $\theta(\eta)$ Fig. 15. Variation of  $\gamma_1$  on  $\phi(\eta)$ Fig. 16. Variation of  $Ec$  on  $\theta(\eta)$ Fig. 17. Variation of  $Ec$  on  $\phi(\eta)$ 

Figure 16 shows the impact of the viscous dissipation on the temperature profile. When the value of the viscous dissipation is increased, the fluid region can store the energy. As a result of dissipation due to fractional heating, heat is generated. Figure 17 display the influence of Eckert number on the concentration profile. It is observed that the concentration of the fluid decreases near the plate. However, it rises away from the surface as the value of the Eckert number is enhanced.

## 5. Conclusion

Concluding all arguments and results we summarized our findings as follows:

The decrement in temperature profile and concentration profile is observed for increasing values of the Prandtl number. It is reported that for enhances increasing values of the thermal radiation  $R$  temperature profile also enhanced. By increasing the thermophoresis parameter  $Nt$  and Brownian motion parameter  $Nb$  concentration boundary layer thickness increases. Physically, heated particles come away from high temperatures as compared to low-temperature so the temperature of fluid increases. Looking at the effect of the chemical reaction, the mass transfer rate is observed to decrease. The temperature profile increases as the Eckert number increases, the physical reason behind it is that an increment in the dissipation enhances the thermal conductivity of the fluid which causes an enhancement in the thermal boundary layer. When  $\gamma_1$  increases, it causes increases in temperature and concentration on the surface which sequels in the thickening of the thermal boundary layer. Numerically, it can be calculated by dividing the convection on the surface to the conduction into the surface of an object. Greater values of Schmidt number  $Sc$  represents the lower mass diffusivity. For the Casson fluid, the higher estimation of the Casson parameter escalates the velocity profile.

## Author Contributions

G. Narender planned the scheme, initiated the project developed the mathematical modeling and conducted the experiments; K. Govardhan analysed the empirical results; G. Sreedhar Sarma examined the theory validation. The manuscript was written through the contribution of all authors. All authors discussed the results, reviewed and approved the final version of the manuscript.

## Acknowledgments

Help by Prof. S.R. Koneru, Retd. Professor, Department of Mathematics, IIT Mumbai in the preparation of this paper is gratefully acknowledged.

## Conflict of Interest

The authors declared no potential conflicts of interest with respect to the research, authorship and publication of this article.

## Funding

The authors received no financial support for the research, authorship and publication of this article.








## References

- [1] L. J. Crane, Flow past a stretching plate, *Zeitschrift für angewandte Mathematik und Physik*, 21(4), 1970, 645-647.
- [2] K. B. Pavlov, Magnetohydrodynamic flow of an incompressible viscous fluid caused by deformation of a plane surface, *Magnitnaya Gidrodinamika*, 4(1), 1974, 146-147.
- [3] T. Fang and J. Zhang, Closed-form exact solutions of MHD viscous flow over a shrinking sheet, *Communications in Nonlinear Science and Numerical Simulation*, 14(7), 2009, 2853-2857.
- [4] H. I. Andersson, K. H. Bech, and B. S. Dandapat, Magnetohydrodynamic flow of a power-law fluid over a stretching sheet, *International Journal of Non-Linear Mechanics*, 27(6), 1992, 929-936.
- [5] K. Bhattacharyya and G. C. Layek, chemically reactive solute distribution in MHD boundary layer flow over a permeable stretching sheet with suction or blowing, *Chemical Engineering Communications*, 197(12), 2010, 1527-1540.
- [6] K. Bhattacharyya, Effects of radiation and heat source/sink on unsteady MHD boundary layer flow and heat transfer over a shrinking sheet with suction/injection, *Frontiers of Chemical Science and Engineering*, 5(3), 2011, 376-384.
- [7] H. Tabaei, M. A. Moghimi, A. Kimiaefar, and M. A. Moghimi, Homotopy analysis and differential quadrature solution of the problem of free-convective magnetohydrodynamic flow over a stretching sheet with the hall effect and mass transfer taken into account, *Journal of Applied Mechanics and Technical Physics*, 52(4), 2011, 624.
- [8] S. P. Anjali Devi, B. Ganga, Effects of viscous and Joules dissipation on MHD flow, heat and mass transfer past a stretching porous surface embedded in a porous medium, *Nonlinear Analysis: Modelling and Control*, 14, 2009, 303-314.
- [9] O. D. Makinde, W. N. Mutuku, Hydromagnetic thermal boundary layer of nanofluids over a convectively heated plate with viscous dissipation and Ohmic heating, *UPB Scientific Bulletin, Series A: Applied Mathematics and Physics*, 76, 2014, 181-192.
- [10] S. E. Ahmed, A. K. Hussein, H. A. Mohammed, S. Sivasankaran, Boundary layer flow and heat transfer due to permeable stretching tube in the presence of heat source/sink utilizing nanofluids, *Applied Mathematics and Computation*, 238, 2014, 149-162.
- [11] S. Akilu, M. Narahari, Effects of heat generation or absorption on free convection flow of a nanofluid past an isothermal inclined plate, *Advanced Materials Research*, 970, 2014, 267-271.
- [12] T. R. Mahapatra and A. S. Gupta, Heat transfer in stagnation-point flow towards a stretching sheet, *Heat and Mass Transfer*, 38(6), 2002, 517-521.
- [13] R. Nazar, N. Amin, D. Filip, and L. Pop, Stagnation point flow of a micropolar fluid towards a stretching sheet, *International Journal of Non-Linear Mechanics*, 39(7), 2004, 1227-1235.
- [14] A. Raptis, C. Perdikis, and H. S. Takhar, Effect of thermal radiation on MHD flow, *Applied Mathematics and Computation*, 153(3), 2004, 645-649.
- [15] A. Ishak, Jafar, R. A. Nazar, and L. Pop, MHD stagnation point flow towards a stretching sheet, *Physica A: Statistical Mechanics and its Applications*, 388(17), 2009, 3377-3383.
- [16] N. S. Akbar, S. Nadeem, R. U. Haq, and Z. H. Khan, Radiation effects on MHD stagnation point flow of nanofluid towards a stretching surface with convective boundary condition, *Chinese Journal of Aeronautics*, 26(6), 2013, 1389-1397.
- [17] R. U. Haq, S. Nadeem, Z. H. Khan, and N. S. Akbar, Thermal radiation and slip effects on MHD stagnation point flow of nanofluid over a stretching sheet, *Physica E: Low-dimensional Systems and Nanostructures*, 65, 2015, 17-23.
- [18] M. Farooq, M. I. Khan, M. Waqas, T. Hayat, A. Alsaedi, and M. I. Khan, MHD stagnation point flow of viscoelastic nanofluid with non-linear radiation effects, *Journal of Molecular Liquids*, 221, 2016, 1097-1103.
- [19] R. K. Dash, K. N. Mehta, and G. Jayaraman, Casson fluid flow in a pipe filled with a homogeneous porous medium, *International Journal of Engineering Science*, 34(10), 1996, 1145-1156.
- [20] J. Venkatesan, D. S. Sankar, K. Hemalatha, and Y. Yatim, Mathematical analysis of Casson fluid model for blood rheology in stenosed narrow arteries, *Journal of Applied Mathematics*, 13, 2013, 1-11.
- [21] T. Hayat, S. A. Shehzad, S. A. Alsaedi, and M. S. Alhothuali, Mixed convection stagnation point flow of Casson fluid with convective boundary conditions, *Chinese Physics Letters*, 29(11), 2012, 114704.
- [22] S. Mukhopadhyay, P. R. De, K. Bhattacharyya, and G. Layek, Casson fluid flow over an unsteady stretching surface, *Ain Shams Engineering Journal*, 4(4), 2013, 933-938.
- [23] S. Mukhopadhyay, Casson fluid flow and heat transfer over a nonlinearly stretching surface, *Chinese Physics B*, 22(7), 2013, 074701.
- [24] S. Nadeem, R. U. Haq, N. S. Akbar, and Z. Khan, MHD three-dimensional Casson fluid flow past a porous linearly stretching sheet, *Alexandria Engineering Journal*, 52(4), 2013, 577-582.
- [25] A. Khalid, I. Khan, A. Khan, and S. Shafie, Unsteady MHD free convection flow of Casson fluid past over an oscillating vertical plate embedded in a porous medium, *Engineering Science and Technology, an International Journal*, 18(3), 2015, 309-317.
- [26] M. I. Khan, M. Waqas, T. Hayat, and A. Alsaedi, A comparative study of Casson fluid with homogeneous-heterogeneous reactions, *Journal of Colloid and Interface Science*, 498, 2017, 85-90.
- [27] Z. Shah, S. Islam, H. Ayaz, and S. Khan, Radiative heat and mass transfer analysis of micropolar nanofluid flow of Casson fluid between two rotating parallel plates with effects of hall current, *Journal of Heat Transfer*, 141(2), 2019, 022401.
- [28] S. Mei, C. Qi, M. Liu, F. Fan, L. Liang, Effects of paralleled magnetic field on thermo-hydraulic performances of Fe<sub>3</sub>O<sub>4</sub>-water nanofluids in a circular tube, *International Journal of Heat and Mass Transfer*, 134, 2019, 704-721.
- [29] C. Qi, T. Luo, M. Liu, F. Fan, Y. Yan, Experimental study on the flow and heat transfer characteristics of nanofluids in double-tube heat exchangers based on thermal efficiency assessment, *Energy Conservation and Management*, 197, 2019, 111870.
- [30] C. Qi, M. Liu, T. Luo, Y. Pan, Z. Rao, Effects of twisted tape structures on thermo-hydraulic performances of nanofluids in a triangular tube, *International Journal of Heat and Mass Transfer*, 127(Part C), 2018, 146-159.
- [31] T. Hayat, M. Bilal Ashraf, S. A. Shehzad, A. Alsaedi, Mixed Convection Flow of Casson Nanofluid over a Stretching Sheet with Convectively Heated Chemical Reaction and Heat Source/Sink, *Journal of Applied Fluid Mechanics*, 8(4), 2015, 803-813.

## ORCID iD

G. Narender  <https://orcid.org/0000-0003-1537-3793>  
 K. Govardhan  <https://orcid.org/0000-0002-6707-3162>  
 G. Sreedhar Sarma  <https://orcid.org/0000-0003-0621-415x>



© 2020 by the authors. Licensee SCU, Ahvaz, Iran. This article is an open access article distributed under the terms and conditions of the Creative Commons Attribution-NonCommercial 4.0 International (CC BY-NC 4.0 license) (<http://creativecommons.org/licenses/by-nc/4.0/>).

How to cite this article: Narender G., Govardhan K., Sreedhar Sarma G. MHD Casson Nanofluid Past a Stretching Sheet with the Effects of Viscous Dissipation, Chemical Reaction and Heat Source/Sink, *J. Appl. Comput. Mech.*, 7(4), 2021, 2040-2048.  
<https://doi.org/10.22055/JACM.2019.14804>

